Biomaterials Science

ROYAL SOCIETY OF CHEMISTRY

PAPER

View Article Online
View Journal | View Issue

Cite this: *Biomater. Sci.*, 2023, **11**, 6600

Acid-sensitive stable polymeric micelle-based oxidative stress nanoamplifier as immunostimulating anticancer nanomedicine†

Gayoung Kwon,[a] Jinsu Baek,[b] Nuri Kim,[a] Soonyoung Kwon,[a] Nanhee Song,[a] Seong-Cheol Park,[c] Byeong-Su Kim[b] and Dongwon Lee*[a,d]

Oxidative stress amplifying compounds could elicit selective killing of cancer cells with minimal toxicity to normal cells and also induce immunogenic cell death (ICD). However, compared to conventional anticancer drugs, oxidative stress amplifying compounds have inferior therapeutic efficacy. It can be postulated that the anticancer therapeutic efficacy and immunostimulating activity of oxidative stress amplifying hybrid prodrug (OSamp) could be fully maximized by employing ultrastable polymeric micelles as drug carriers. In this work, we developed tumour-targeted oxidative stress nanoamplifiers, composed of OSamp, amphiphilic poly(ethylene glycol) methyl ether-*block*-poly(cyclohexyloxy ethyl glycidyl ether)s (mPEG–PCHGE) and a lipopeptide containing Arg–Gly–Asp (RGD). Tumour targeted OSamp-loaded mPEG–PCHGE (T-POS) micelles exhibited excellent colloidal stability and significant cytotoxicity to cancer cells with the expression of DAMPs (damage-associated molecular patterns). In the syngeneic mouse tumour model, T-POS micelles induced significant apoptotic cell death to inhibit tumour growth without noticeable body weight changes. T-POS micelles also induced ICD and activated adaptive immune responses by increasing the populations of cytotoxic $CD4^+$ and $CD8^+$ T cells. Therefore, these results suggest that T-POS micelles hold great translational potential as immunostimulating anticancer nanomedicine.

Received 5th May 2023,
Accepted 14th August 2023

DOI: 10.1039/d3bm00770g

rsc.li/biomaterials-science

Introduction

Chemotherapy is the use of powerful chemical drugs to destroy cancer cells and has been most often utilized to treat tumours over the last couple of decades. However, there are considerable limitations such as their low bioavailability and off-target toxicity. To address these limitations, it is necessary to understand the characteristic environment of cancer cells compared with normal cells. Unlike normal cells, cancer cells have active metabolism and produce excessive ROS such as H_2O_2 for fast growth and proliferation.[1,2] To counterbalance the detrimental effects of ROS overproduction, cancer cells are well equipped with large amounts of antioxidants such as glutathione (GSH).[3,4] In this context, cancer cells are characterized by the altered redox balance and are therefore more vulnerable to oxidative stress, which provides a valuable cue for oxidative anticancer therapy.[5,6] It has been well accepted that ROS overaccumulation, antioxidant depletion and/or their combination could kill cancer cells with minimal toxicity to normal cells.[7,8] Furthermore, cancer therapy induced by oxidative stress elevation is known to induce ICD.[9] ICD is characterized by active or passive expression of DAMPs including high mobility group box 1 (HMGB1) and calreticulin (CRT). In particular, DAMPs expressed from damaged cells stimulate antigen presenting cells such as dendritic cells and activate T cells, leading to potent immune responses.[10] On the basis of these biochemical characteristics in cancer cells, there has been increasing interest in developing strategies that specifically amplify oxidative stress in cancer cells to exert anticancer effects and immunostimulating activity.[11,12]

In the previous study, we reported a hybrid anticancer agent, termed OSamp, which consists of ROS generating cinnamaldehyde and GSH depleting quinone methide (QM).[11] OSamp undergoes acid- and esterase-catalysed hydrolysis to generate ROS and scavenge GSH, simultaneously, leading to oxidative stress amplification. OSamp could significantly

[a]*Department of Bionanotechnology and Bioconvergence Engineering, Jeonbuk National University, Jeonju, Jeonbuk 54896, Korea*
[b]*Department of Chemistry, Yonsei University, Seoul, 03722, Korea*
[c]*Department of Polymer Engineering, Sunchon National University, Chonnam 57922, Korea*
[d]*Department of Polymer Nano Science and Technology, Jeonbuk National University, Jeonju, Jeonbuk 54896, Korea*

† Electronic supplementary information (ESI) available. See DOI: https://doi.org/10.1039/d3bm00770g

elevate oxidative stress to induce apoptotic cell death through mitochondrial disruption, cytochrome *c* release and activation of apoptosis-related genes. Despite its great potential as an anticancer therapeutic agent with minimized toxicity proven in the tumour xenograft model, the clinical translation of OSamp is hampered by its lower therapeutic efficacy compared to conventional anticancer drugs. Moreover, the potential immunogenic activity of OSamp has not been explored yet. We therefore reasoned that the therapeutic potential and immunostimulating activity of OSamp could be fully maximized by the use of drug carriers that could have high drug loading capacity, target cancer cells specifically and release drug payloads in a spatiotemporally controlled manner.[13]

Various drug carriers have been extensively explored for the delivery of hydrophobic drugs and biologics such as proteins and nucleic acid. Among numerous drug carriers, amphiphilic polymeric micelles possess highly suitable and desirable properties for drug delivery such as small size, unique nanoscopic architecture, stability and the facile fabrication.[14] Based on these advantages, various types of polymeric micelles have been developed including pH-responsive, ROS-sensitive, electric field-reactive micelles, *etc.*, by adding additional functional moieties to the backbone or side chains of polymers.[15] In the design of amphiphilic polymer micelles, the selection of hydrophobic moiety is of primary importance because the hydrophobic interaction is the major driving force for micelle formation through self-assembly. In general, the increment of hydrophobicity enhances the drug loading capacity, loading efficiency and stability.[16,17] Upon contact with biological environment, proteins adsorb on the surface of micelles non-specifically to reduce their colloidal stability, deteriorating the drug delivery efficacy.[18] In this regard, it is critical to develop amphiphilic polymer that has sufficient hydrophobic interactions to generate micelles with high drug loading capacity and efficiency. In the previous study, Son *et al.* developed amphiphilic block copolymer mPEG–PCHGE that contains an acid-cleavable hydrophobic acetal linkage and self-assembles to form stable micelles under aqueous conditions.[18] The PCHGE micelles possess the excellent stability, encapsulation efficiency, acid-triggered drug release kinetics, and acceptable biocompatibility as a potential drug delivery carrier.

Integrin is a cell adhesion molecule that is overexpressed on the surface of various cancer cell membranes and has been widely recognized as a tumour biomarker.[19] As integrin is well known to have high affinity to a peptide, Arg–Gly–Asp (RGD), a lipopeptide, 1,2-distearoyl-*sn-glycero*-3-phosphoethanolamine (DSPE)-PEG–RGD, has been widely explored to refine the surface of drug carriers to realize tumour targeted drug delivery.[20] It could be therefore expected that amphiphilic mPEG–PCHGE and DSPE-PEG–RGD could self-assemble under the aqueous condition to form micelles that could encapsulate drug payloads and deliver them to the tumour site specifically. In this study, we postulated that the therapeutic efficacy and immunostimulating activity of OSamp could be fully maximized by tumour targeting RGD-decorated mPEG–PCHGE micelles. Tumour targeting OSamp-loaded mPEG–PCHGE (T-POS) micelles were expected to target cancer cells preferentially and release OSamp in the acidic environment to amplify oxidative stress, leading to strong ICD (Scheme 1). To verify this concept, the biophysical properties of T-POS micelles were

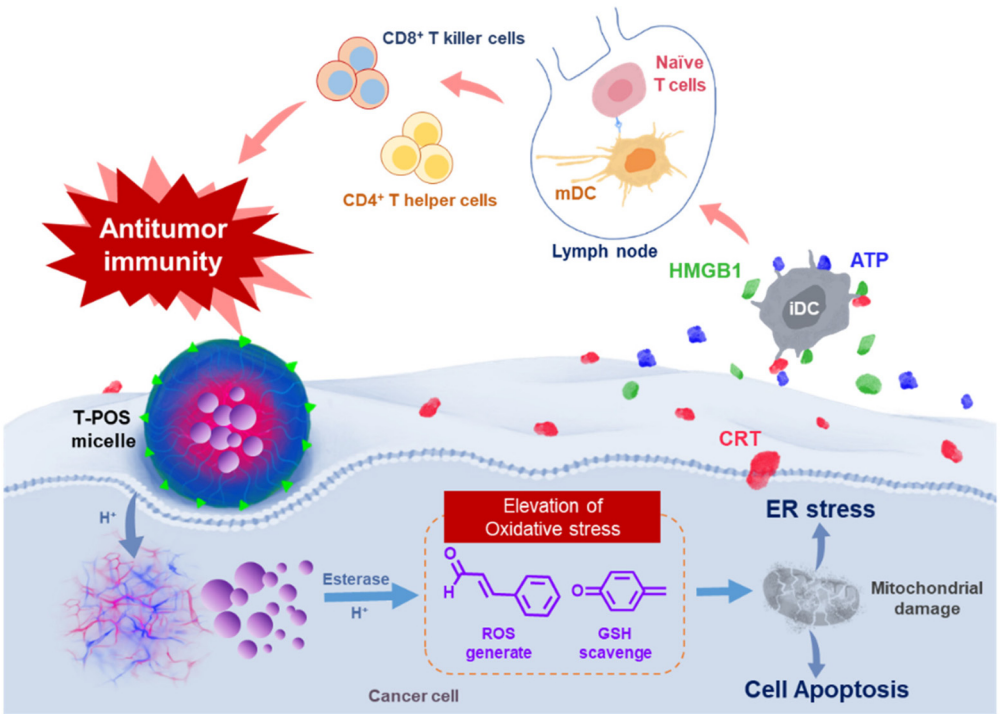

Scheme 1 The proposed mechanism of T-POS micelles as a targeted effective oxidative stress nanoamplifier and ICD inducer for cancer therapy.

extensively studied and their anticancer therapeutic effects were evaluated using cell culture models and syngeneic mouse tumour models. The findings in this study suggest that T-POS micelles hold promising translational potential as tumour-targeted anticancer nanomedicine.

Results and discussion

Characterization of T-POS micelles

Synthesis and characterization of OSamp are shown in Fig. S1–S5.† Fig. S6† shows the structure and synthetic route of mPEG–PCHGE. mPEG–PCHGE and DSPE-PEG–RGD (Fig. S7†) self-assembled to form stable T-POS micelles (Fig. 1a), in which OSamp was physically encapsulated. The content of OSamp in T-POS micelles was determined to be ~10 wt%. T-POS micelles were nanospheres with a mean hydrodynamic diameter of ~180 nm (Fig. 1b), determined by TEM and dynamic light scattering. The surface charge of T-POS micelles was determined by measuring their zeta potential in PBS (phosphate buffered saline) at pH 7.4. While OSamp loaded mPEG–PCHGE (POS) micelles exhibited 13 mV, T-POS micelles showed significantly lower zeta potential, 0.45 mV (Fig. 1c). The lower zeta potential of T-POS micelles can be explained by the presence of aspartic acid in RGD which has a negative charge.[21] These results also support that DSPE-PEG–RGD is incorporated in T-POS micelles and RGD protrudes outward to serve as a cancer cell targeting ligand.

Upon intravenous administration, micelles face several challenges such as significant dilution in the bloodstream and non-specific adsorption of blood components including albumin and apolipoproteins, which shifts the micellar equilibrium toward the unimer state.[22] Micelles are therefore subjected to premature disintegration in systemic circulation, which negates delivery efficacy and creates toxicity concerns.[23] As the stability of micelles as a drug carrier is a critical parameter determining the drug delivery efficiency and is greatly influenced by the biological environment, the colloidal stability of T-POS micelles was examined by measuring their hydrodynamic diameter during the incubation with fetal bovine serum (FBS). Because of a large extent of light scattering by 100% FBS which is highly viscous liquid, T-POS micelles were incubated with 70 wt% FBS. As shown in Fig. 1d, T-POS micelles exhibited no or negligible changes in their hydrodynamic diameter for 6 days of observation even in the presence of FBS as high as 70%, suggesting that T-POS micelles would be highly stable in the physiological environment. The excellent colloidal stability of T-POS micelles could be explained by the sufficient hydrophobicity of cyclic acetal moieties of PCHGE. As previously reported, strong hydrophobic interactions in the core of micelles could contribute to the significantly low critical micelle concentration value, ~2 μg mL^{-1}.[18]

We also investigated the acid-responsiveness of T-POS micelles. After the addition of HCl solution, the diameter of T-POS micelles dramatically increased, indicating the micellar dissociation. The acid-responsiveness of T-POS micelles is attributed solely to the acid-triggered cleavage of acetal linkages and subsequent hydrophobic-to-hydrophilic transition of PCHGE (Fig. S8†). Acid-responsive drug release of T-POS micelles was investigated using Nile red-loaded T-PCHGE micelles. Because OSamp readily degrades in acid-triggered manner, Nile red was loaded as a model drug, whose fluorescence is strongly influenced by the polarity of the environment. The micelles exhibited strong fluorescence at pH 7.4, indicating that Nile red is encapsulated in the hydrophobic core of micelles (Fig. 1e).

However, at pH 5.0, the fluorescence intensity rapidly decreased because Nile red was released from the micelles and

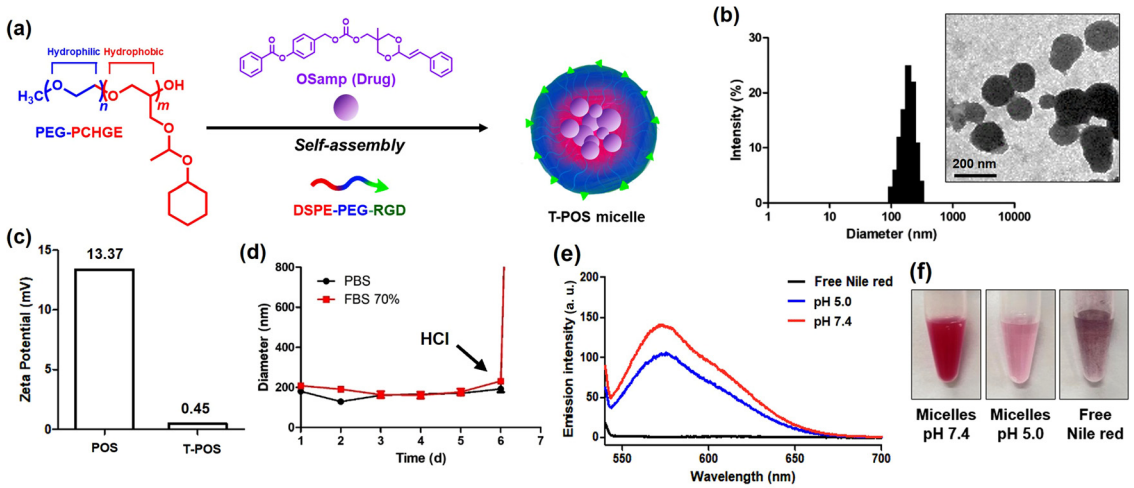

Fig. 1 Characterization of T-POS micelles. (a) A schematic of T-POS micelles formulation. (b) Size distribution of T-POS micelles determined by dynamic light scattering. The inset is the TEM image. (c) Zeta potential of T-POS micelles dispersed in PBS. (d) Changes in the hydrodynamic diameter of T-POS micelles during the incubation in PBS and 70% (v/v) FBS. (e) Fluorescence emission spectra of Nile red encapsulated in T-POS micelles after excitation at a wavelength of 530 nm. (f) Photographs of Nile red-loaded T-PCHGE micelles at pH 5.0 and 7.4.

lost fluorescence into the aqueous environment. Nile red-loaded T-PCHGE micelles showed strong red colour at pH 7.4. In contrast, the red colour of the micelles faded markedly at pH 5.0 (Fig. 1f). These results suggest that T-PCHGE micelles could release the drug payloads in an acid-triggered manner and are in good accordance with our previous study that reports the pH-dependent drug release kinetics of PCHGE micelles.[18]

Cellular uptake and endosomal escape of T-PCHGE micelles

The cellular uptake and endosomal escape ability of T-PCHGE micelles were examined using a fluorescent reporter and fluorescence microscope. Fluorescent IR780 was used as a red fluorescent probe for T-PCHGE micelles and LysoTracker was utilized as a lysosomal probe to investigate the endo/lysosomal escape of T-PCHGE micelles. CT26 cells were incubated with IR780-loaded T-PCHGE micelles and then stained with LysoTracker. Discernible red fluorescence was observed in cells after 3 h incubation and the intensity increased with time (Fig. 2a), indicating the internalization of T-PCHGE micelles. At 3 h-post incubation, green fluorescence was also observed and cells showed yellow fluorescence because of the co-localization of IR780-loaded T-PCHGE micelles and LysoTracker in the acidic compartments such as endosomes and lysosomes, suggesting that these compartments are intact. However, at 6 h post-incubation, green signal markedly decreased because LysoTracker was released into neutral cytosol and lost fluorescence. After 12 h, only red fluorescence was observed in the cytoplasm, indicating the rupture of the acidic compartments. These observations suggest that T-PCHGE micelles are readily taken up by cells and disintegrated in the acidic environment, leading to the rupture of endo/lysosomes and subsequent drug release to the cytoplasm. The endo–lysosomal escape of T-PCHGE micelles could be explained by the osmotic pressure buildup in the acidic endo/lysosomes resulting from the acid-triggered degradation of PCHGE and subsequent release cyclohexanol and aldehyde.[18,24]

We also investigated the effects of RGD on the cellular uptake of T-PCHGE micelles. T-PCHGE micelles incorporating RGD showed higher red fluorescence than PCHGE micelles without RGD (Fig. 2b). This suggests that RGD on the surface enhances the cellular uptake of micelles. However, in the presence of free RGD, cellular uptake was markedly reduced. These findings demonstrate that the cellular uptake of T-PCHGE micelles greatly depend on RGD.

Blood compatibility and cytotoxicity of T-POS micelles

As blood is the first contact for nanoparticles injected intravenously and blood compatibility is one of major criteria limiting the clinical applications of blood-contacting materials such as drug carriers,[25] we performed hemolysis assay to evaluate the hemocompatibility of T-PCHGE micelles.

Plasma containing erythrocytes were incubated with T-PCHGE micelles for 24 h and the concentration of haemoglobin released from erythrocytes was determined. As shown in Fig. 3a and b, T-PCHGE micelles induced no erythrocyte destruction, evidenced by the negligible change in the level of haemoglobin. These findings suggest that T-PCHGE micelles have excellent blood compatibility.

Next, MTT assay was performed to evaluate the cytotoxicity of T-POS micelles against CT26 cells. T-POS micelles showed concentration-dependent cytotoxicity against CT26 cells. The cell viability was decreased to 15% by 150 μg mL^{-1} of T-POS micelles. The cytotoxicity of T-POS micelles was almost the same as those of the equivalent free OSamp (Fig. 3c). The results suggest that upon cellular uptake, stable acid-responsive T-POS micelles release OSamp completely in the cytosol through effective endo–lysosomal escape and the carriers

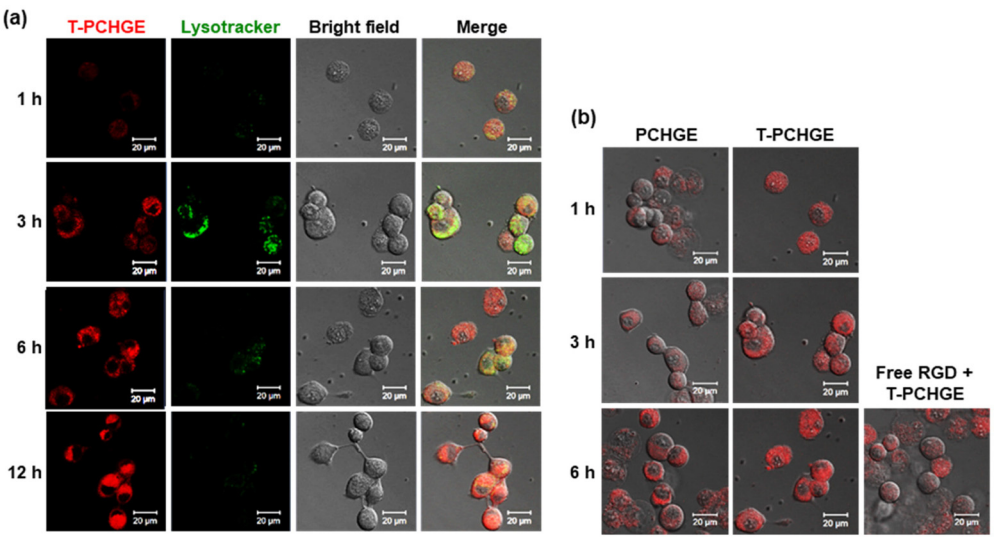

Fig. 2 Cellular uptake and endosomal escape of T-PCHGE micelles. (a) Fluorescence images of CT26 cells treated with IR780-loaded T-PCHGE micelles. LysoTracker Green was used to stain acidic compartments. (b) Fluorescence images of CT26 cells treated with IR780-loaded T-PCHGE micelles in the presence or absence of free RGD.

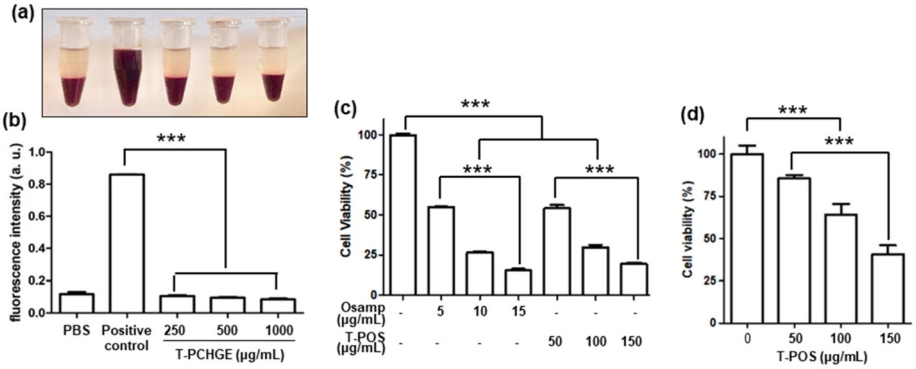

Fig. 3 Hemocompatibility and cytotoxicity of T-POS micelles. (a) Photographs of plasma treated with various concentration of T-PCHGE micelles. (b) The level of hemoglobin released in plasma. Viability of (c) CT26 and (d) RAW 264.7 cells treated with T-POS micelles. Values are presented as the mean ± SD. ***$p < 0.001$ (one-way ANOVA with Tukey's *post hoc* test; $n = 6$).

would not negate the cytotoxicity of OSamp. Not surprisingly, T-POS micelles exerted less cytotoxicity against normal cells, RAW 264.7 cells compared to CT26 cells (Fig. 3d). The superior toxicity of T-POS micelles against cancer cells could be explained by the biological differences between cancer cells and normal cells. Oxidative stress amplifying T-POS micelles could significantly elevate oxidative stress to kill cancer cells preferentially.

ICD induction by T-POS micelles

As oxidative stress amplifying OSamp was reported to induce apoptotic cell death through mitochondrial damages and ICD is a form of apoptosis induced by oxidative stress inducing chemotherapeutic drugs,[26] we assessed the ability of T-POS micelles to induce ICD. One of the major features of ICD is the exposure on the cell membrane or secretion of DAMPs family such as HMGB1 and CRT, which stimulates the host immune system and enhances immunological responses.[12,27,28] CRT mainly located in the lumen of the endoplasmic reticulum (ER) is translocated to the cell surface by ROS-mediated ER stress in the early apoptotic stage. CRT is a key feature determining anticancer immune responses by serving as an "eat me" signal to deliver the activation of a phagocytosis signal.[12,29,30] We first investigated the effects of T-POS micelles on the surface exposure of CRT by immunofluorescence staining which is considered as a golden standard to estimate ICD induction.[31] As shown in the Fig. 4a, T-POS micelles increased

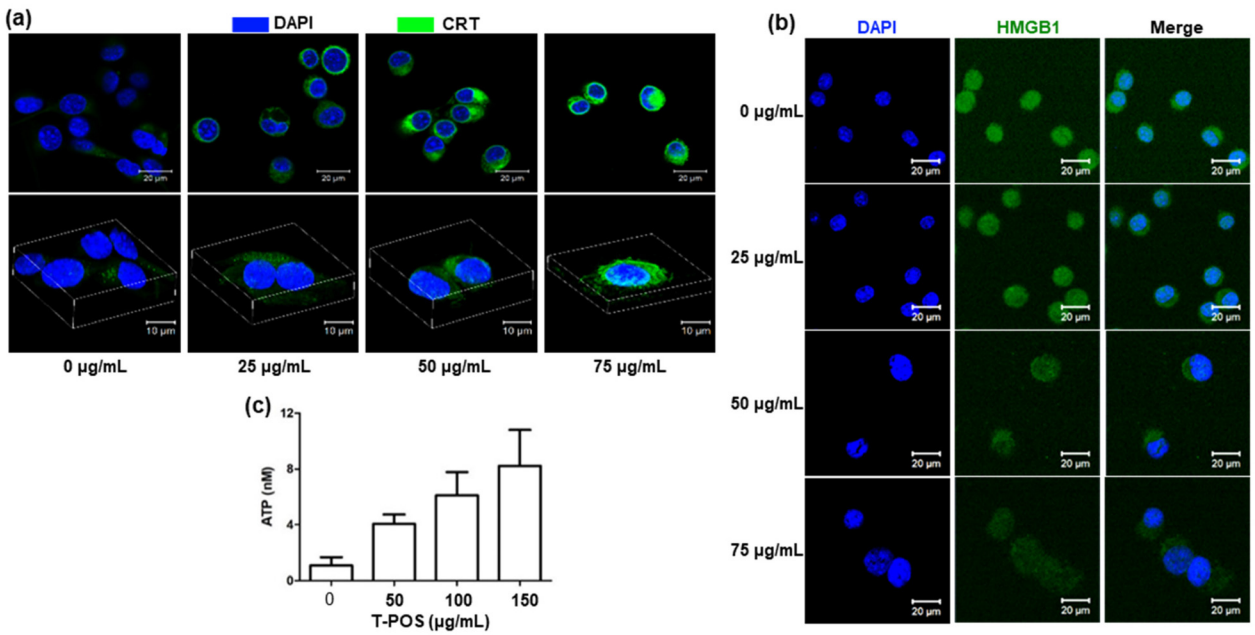

Fig. 4 Induction of ICD by T-POS micelles. (a) Fluorescence images showing the CRT exposure on the surface of CT26 cells. The bottom panel shows the 3D fluorescence imaging of cells. (b) Fluorescence images showing HMGB1 in the cytosol of CT26 cells. (c) The extracellular level of ATP after 24 h of treatment with T-POS micelles. Values are presented as the mean ± SD. ***$p < 0.001$ ($n = 4$).

the surface exposure of CRT concentration-dependently. HMGB1 is a non-histone chromatin-binding protein, playing essential roles in transcription and is translocated to the cytosol and extracellular environments in the late apoptosis to serve as a pro-inflammatory cytokine to promote antigen presentation.[32]

In the untreated cells, HMGB1 was predominantly observed in the nucleus, evidenced by the nucleus DAPI staining (Fig. 4b). However, T-POS micelles increased the level of HMGB1 released in cytosol, in a concentration dependent manner. As adenosine triphosphate (ATP) is another important hallmark of ICD and the release of ATP from dying cells occurs independently of CRT exposure and HMGB1 release,[33] the level of ATP released in culture medium was measured after 24 h of treatment with T-POS micelles. T-POS micelles significantly increased the level of extracellular ATP (Fig. 4c). Taken all, as oxidative stress nanoamplifiers, T-POS micelles induce strong ICD which could exert potent immunostimulating activity.

In vivo and *ex vivo* antitumour effects of T-POS micelles

The *in vivo* antitumour effects of T-POS micelles were evaluated using the syngeneic mouse model. CT26 cells were inoculated into BALB/c mice to establish tumours. Since RGD is known to target integrin overexpressed on the membrane of various cancer cells, we first examined the ability of T-POS micelles to target tumours. For fluorescence imaging, IR780 was loaded in micelles instead of OSamp and CT26 tumour-bearing mice were injected with the fluorescent micelles. Fig. 5a shows the fluorescence images of CT26 tumour-bearing mice after the injection of PCHGE or T-PCHGE micelles loaded with IR780. From 6 h after injection, tumours showed discernible fluorescence signal. PCHGE micelles without RGD targeting ligand could preferentially accumulate in tumours due to the

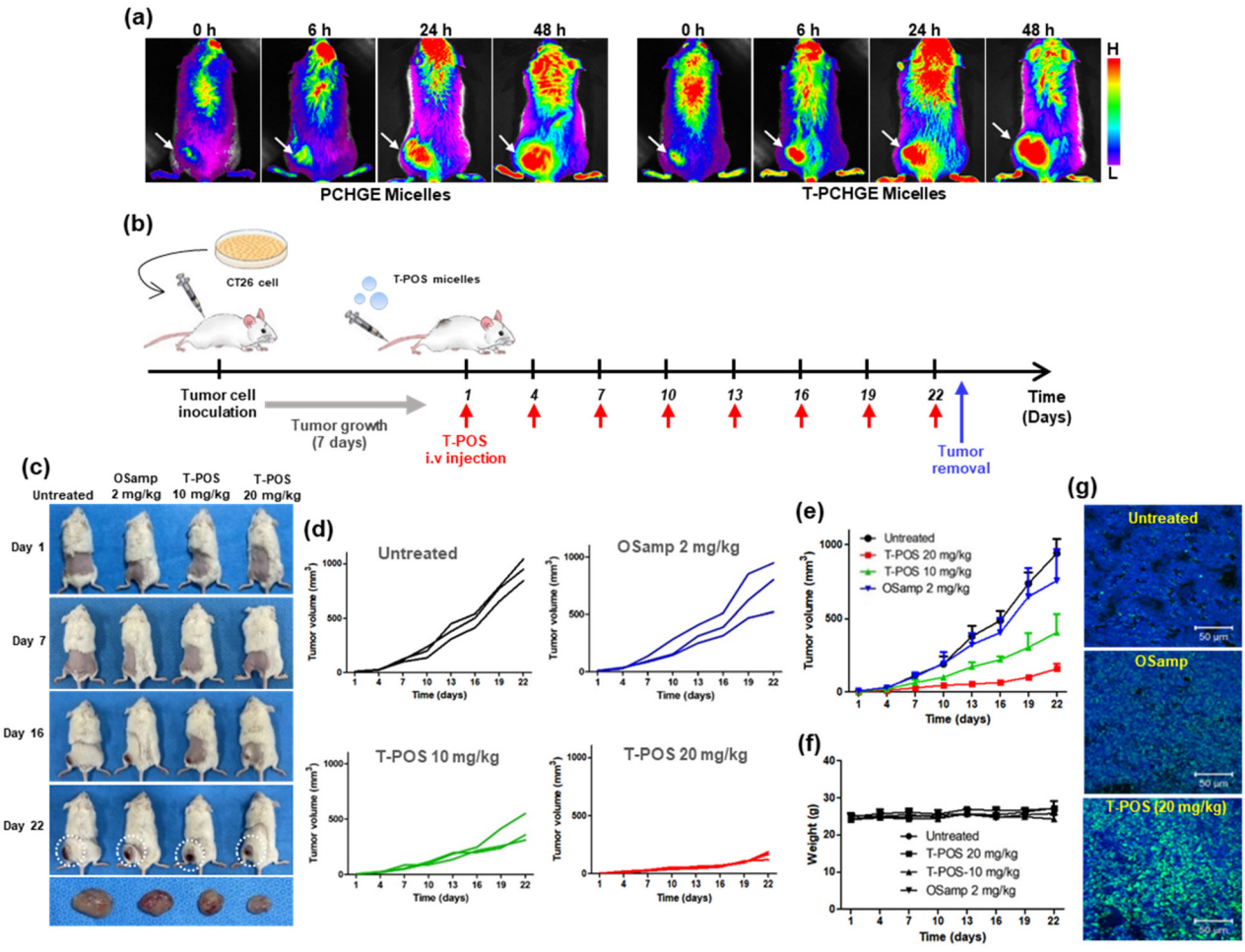

Fig. 5 Evaluation of anticancer activity of T-POS micelles using syngeneic mouse tumour models. (a) Fluorescence images of tumour bearing mice after injection of PCHGE or T-PCHGE micelles loaded with IR780 at various time points. Arrows indicate the tumour site. (b) Experimental time line for syngeneic mouse model. (c) Photographs of tumour bearing mice during the treatment. (d) Monitoring of tumour volumes during the treatment with OSamp and T-POS micelles. (e) Comparison in suppressive effects in tumour growth. (f) Changes in body weight during the treatment. Values are presented as the mean ± SD. (g) Representative fluorescence images of tumour tissues stained with TUNEL. Green: TUNEL; blue: DAPI.

enhanced permeation and retention (EPR) effects resulting from their small size and superior stability. Not surprisingly, T-PCHGE micelles could accumulate in tumours more profoundly than PCHGE micelles, indicating that RGD incorporated in micelles plays a critical role in tumour targeting.

To assess the anticancer activity of T-POS micelles, when tumours reached a volume of ~50 mm^3, mice were injected with OSamp (2 mg kg^{-1}) and T-POS micelles (10 or 20 mg kg^{-1}) through intravenous injection. OSamp or T-POS micelles were given every 3 days and tumour volumes and body weight were monitored for 22 days (Fig. 5b). The tumour volume of untreated mice increased continuously and gradually. OSamp without vehicles showed marginal antitumour effect. However, RGD-decorated stable polymer micelles significantly increased the therapeutic efficacy of OSamp. As shown in Fig. 5c–e, T-POS micelles at a dose of 20 mg kg^{-1} exerted significantly higher anticancer effects than the equivalent dose (2 mg kg^{-1}) of OSamp. No noticeable changes in body weight were observed during the treatment (Fig. 5f). We also found that T-POS micelles induced apoptotic cell death more profoundly than the equivalent OSamp, evidenced by TUNEL staining (Fig. 5g & S9†). During the treatment, T-POS micelles induced no changes in the body weight during the treatment. These findings strongly demonstrate that the therapeutic effects of OSamp was significantly enhanced by tumour targeting stable polymer (T-PCHGE) micelles.

Immunogenic activity of T-POS micelles

To assess whether T-POS micelles induce ICD to elicit antitumour immune responses, we examined the levels of proinflammatory cytokine and DAMPs by immunofluorescence imaging of tumour tissues. We first investigated the level of tumour necrosis factor-alpha (TNF-α) in tumour tissues because TNF-α is known to be released from dying cancer cells to promote anticancer immune responses. The group treated with T-POS micelles showed a significantly increased level of TNF-α compared to other groups (Fig. S10†). T-POS micelles markedly increased the surface exposure of CRT more profoundly the equivalent OSamp (Fig. 6a & S11a†). T-POS micelles also enhanced the extracellular release of HMGB1, evidenced by the remarkable decrease in green fluorescence (Fig. 6b & S11b†). These findings are in good accordance with the results of *in vitro* studies (Fig. 4a and b).

As a danger signal, DAMPs including CRT and HMGB1 are known to activate the adaptive immune responses, which is characterized by the proliferation of cytotoxic T lymphocyte ($CD4^+$ and $CD8^+$ T cells) against cancer cells.[28,34] To further support enhanced immune responses by ICD-inducing T-POS

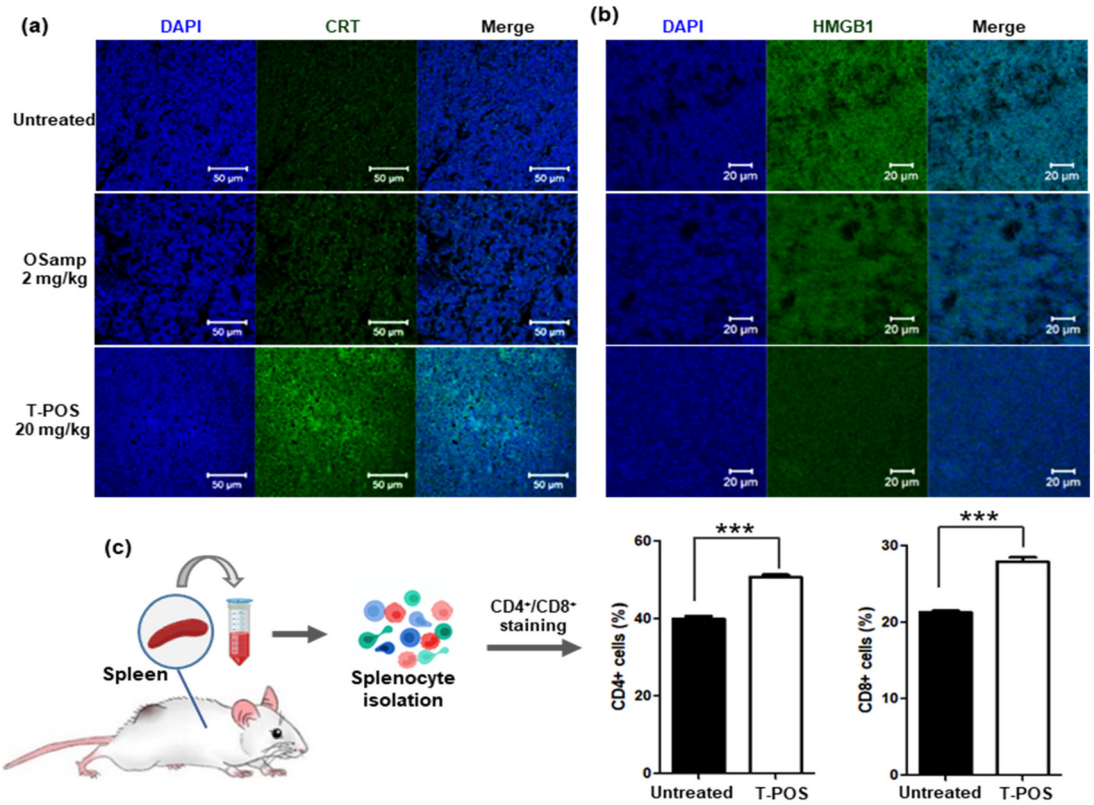

Fig. 6 ICD induction by T-POS micelles. (a) Fluorescence images of tumour tissues stained with (a) anti CRT and (b) anti HMGB1 antibody labelled with Alexa Fluor 488. (c) Flow cytometric analysis of $CD4^+$ and $CD8^+$ T cells in spleen lysates after the T-POS micelles treatment. Values are as the mean ± SD (n = 3). ***p < 0.001. One-way ANOVA with Tukey's *post hoc* test.

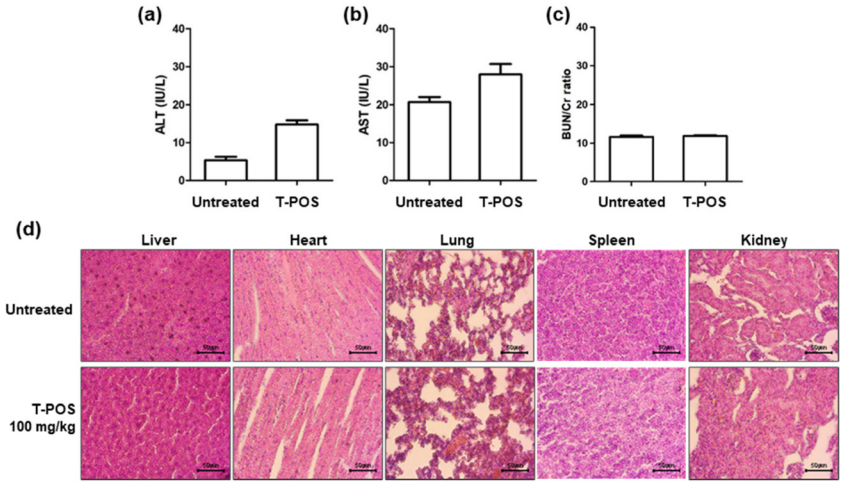

Fig. 7 Biosafety of T-POS micelles. The serum level of (a) ALT and (b) AST. (c) The ratio between BUN and creatinine (Cr) in the serum. Values are presented as the mean ± SD (n = 3). (d) Histological examination of major organ tissues stained with H&E.

micelles, we investigated the populations of $CD4^+$ and $CD8^+$ T cells in spleen which plays a significant role in adaptive immunity as a lymphatic organ.[35] At 12 day-post T-POS micelles treatment, the populations of cytotoxic splenic $CD4^+$ and $CD8^+$ T cells were significantly increased compared to the untreated group (Fig. 6c), attributed largely to the oxidative stress amplification, CRT translocation and HMGB1 release.[36] These results demonstrate that T-POS micelles effectively induce ICD to promote T cell activation, eliciting antitumour immune activity.

The primary objective of this study was to demonstrate that the anticancer therapeutic efficacy of oxidative stress amplifying OSamp could be enhanced by RGD-decorated acid-responsive stable polymer micelles. In the proof-of-concept study using syngeneic mouse tumour models, T-POS micelles induced strong ICD to elicit anticancer immune activity. However, further studies are warranted to fully elucidate the ability of T-POS micelles to induce ICD by determining the maturation of antigen presenting cells such as dendritic cells, T cell activation/proliferation, T cell recruitment and infiltration into tumours, and the level of pro-inflammatory cytokines.

Biosafety of T-POS micelles

To investigate the biosafety, normal mice were treated with T-POS micelles at a dose of 100 mg kg^{-1}, 5-fold higher than those of *in vivo* anticancer studies. The levels of alanine transamidase (ALT) and aspartate transaminase (AST) were slightly increased after the treatment with T-POS micelles. However, the serum levels of ALT and AST remained in the normal range (Fig. 7a and b). In addition, no significant changes were observed in the level of renal index such as creatinine and blood urea nitrogen (BUN) (Fig. 7c). Histological examination of major organ tissues also revealed that no abnormal histological damages were induced by T-POS micelles (Fig. 7d). These results demonstrate that T-POS micelles induce no noticeable changes in renal and hepatic functions and have acceptable biocompatibility for clinical translation.

Conclusions

Oxidative stress nanoamplifiers (T-POS micelles) composed of OSamp, amphiphilic mPEG–PCHGE block copolymer, and lipopeptide (DSPE-PEG–RGD) were developed as anticancer nanomedicine with immunostimulating activity. T-POS micelles showed excellent stability in the physiological environment and could be effectively taken up by cancer cells through RGD-mediated endocytosis. T-POS micelles exerted cancer cell-preferential cytotoxicity and also induced ICD, evidenced by the surface exposure of CRT and release of HMGB1 and ATP. In syngeneic mouse tumour models, the RGD-decorated micelles preferentially accumulated in the tumour environment and released OSamp to inhibit tumour growth. In addition, T-POS micelles induced ICD to elicit antitumour immune activity, evidenced by the release of CRT and HMGB1 and the enhanced cytotoxic T cell activation. The results demonstrate that therapeutic efficacy of OSamp could be significantly enhanced by tumour targeting stable polymer micelles. Given their acid-responsiveness, colloidal stability, cancer cell-preferential cytotoxicity and anticancer immune activity, oxidative stress amplifying T-POS micelles have tremendous potential as anticancer nanomedicine with immunostimulating activity.

Experimental

Materials

4-Hydroxybenzoic acid, benzoyl chloride, cinnamaldehyde, 1,1,1-tris(hydroxymethyl)ethane, 4-(dimethylamino)pyridine, 1,1′-carbonyldiimidazole were obtained from Sigma-Aldrich (St Louis, MO, USA). Trimethylamine was obtained from

Junsei (Japan). *p*-Toluene sulfonic acid was obtained from TCI (Japan). Dichloromethane (DCM), tetrahydrofuran (THF), ethyl acetate and hexane were obtained from Samchun (Korea). mPEG–PCHGE was synthesized as previously reported.[18]

Synthesis of OSamp

OSamp was synthesized as previously reported (Fig. S1†).[11] 4-Hydroxybenzyl alcohol (5.0 g, 40.9 mmol) and benzoyl chloride (5.7 g, 40.9 mmol) were dissolved in 200 mL of anhydrous THF. Trimethylamine (5.7 mL, 40.9 mmol) was added dropwise to the solution in an ice bath. The solution was stirred for 30 min in an ice bath and left at room temperature for 12 h. After phase separation, only the organic phase was obtained by filtering. The remaining solvent was evaporated and the compound **1** was obtained (75% yield) using column chromatography on silica gel (ethyl acetate/hexane = 1/2) (Fig. S2†). 1,1,1-Tris(hydroxymethyl)ethane (5.0 g, 41.6 mmol), cinnamaldehyde (5.2 mL, 41.6 mmol) and *p*-toluene sulfonic acid (1.8 g, 10.4 mmol) were dissolved in 200 mL of anhydrous DCM. The reaction was allowed for 12 h at 75 °C. After cooling down to room temperature, the reaction was terminated by adding 1 mL of trimethylamine. The solvent was removed using a rotary evaporator and the compound **2** was purified (60% yield) by column chromatography in silica gel (ethyl acetate/hexane = 2/5) (Fig. S3†). **2** (2.0 g, 8.5 mmol) was reacted with 1,1′-carbonyldiimidazole (2.7 g, 17.0 mmol) in 100 mL of anhydrous DCM for 30 min at room temperature. The solvent was evaporated and the compound **3** was obtained (90% yield) from column chromatography using ethyl acetate in silica gel (Fig. S4†). **3** (2.0 g, 6.1 mmol) and **1** (1.7 g, 7.3 mmol) were dissolved in 50 mL of anhydrous DCM containing 4-(dimethylamino)pyridine (0.7 g, 6.1 mmol). The reaction was allowed at 45 °C to obtain OSamp (Fig. S5†), 4-(((((5-methyl-2-stytyl-1,3-dioxan-5-yl)methoxy)carbonyl)oxy)methyl)phenyl benzoate for 48 h. OSamp was purified (40% yield) by column chromatography in silica gel (ethyl acetate/hexane = 1/2).

Formulation and characterization of T-POS micelles

mPEG-PCHGE (1.9 mg) and OSamp (0.1 mg) were dissolved in 100 μL anhydrous THF and DSPE-PEG–RGD (0.1 mg) was dissolved in 50 μL phosphate buffered saline (PBS). Two solutions were gently mixed. The mixture was added dropwise to the (1.0 mL) PBS at pH 7.4. Remaining THF was eliminated under high vacuum, and 2 mg mL^{-1} concentration of T-POS micelles were obtained. The morphology of micelles was investigated using a transmission electron microscope (Bio-TEM, HITACHI Corp., Japan) after negative staining with phosphotungstic acid solution. The size of micelles was analysed using a particle size analyser (90Plus, Brookhaven Instrument Corp., Holtsville, NY).

Stability of T-POS micelles

T-POS micelles were formed at PBS (pH 7.4) containing 70 vol% fetal bovine serum (FBS), a condition that is similar to the biological environment. The hydrodynamic diameter of T-POS micelles was measured for 120 h using a particle size analyser. After 120 h, the pH-responsive degradation was confirmed by adding hydrochloride acid to micelles.

Blood compatibility of T-POS micelles

Blood from normal mice was centrifuged to collect plasma. Plasma was treated with T-POS micelles (250, 500, 1000 μg mL^{-1}) and incubated for 24 h at room temperature. As a positive control, 0.1% sodium dodecylsulfate (SDS) was used. UV absorbance at 405 nm of the plasma was measured using a UV-vis (Scinco, Korea).

pH-Responsive release kinetics of T-POS micelles

The T-PCHGE micelles loaded with Nile red was incubated in phosphate buffer (pH 7.4) solution at room temperature. pH was adjusted to pH 5.0 by adding HCl solution (10 M). The fluorescence spectrometer (FP-6500, Jasco, Japan) was used to verify the pH-responsive release of Nile red from T-POS micelles.

Cell culture

Mouse colon adenocarcinoma cell line (CT26) and mouse macrophage cell line (RAW 264.7) were obtained from Korean Cell Line Bank (Seoul, Korea). Cells were cultured using DMEM medium with 10% FBS and incubated at 37 °C with 5% CO_2.

Cellular uptake and endosomal escape of T-POS micelles

CT26 cells were seeded in a glass bottomed dish at a density of 3×10^5 cells per dish. After incubation overnight, cells were treated with IR780-loaded T-PCHGE micelles (100 μg mL^{-1}) for 1, 3, 6 and 12 h. After treatments of T-PCHGE micelles, cells were treated with LysoTracker for 45 min to stain endosomes and lysosomes. Cells were gently washed with fresh medium, and fluorescence images of cells were obtained by using a confocal laser scanning microscope (CLSM 510 Meta, Carl Zeiss, Inc., Germany).

Cytotoxicity of T-POS micelles

CT26 cells RAW 264.7 cells were incubated with various concentration of T-POS micelles for 24 h. Cells were treated with MTT (3-(4,5-dimethylthiazol-2-yl)-2,5-diphenyltetarazolium bromide) solution (100 μL). Following the incubation for 3 h, 1 mL of dimethyl sulfoxide (DMSO) was added to cells to dissolve the generated formazan crystals. The absorbance of cells at 570 nm was measured by using a microplate reader (Biotek Instruments, Winooski, VT, USA) to verify the cell viability.

Evaluation of cell surface externalized CRT

The surface exposure of CRT was verified by using a confocal laser scanning microscope (CLSM). CT26 cells were seeded in the glass bottom dish at a density of 3×10^5 cells per dish and incubated for 24 h. Cells were treated with various concentration of T-POS micelles for 12 h. Then the cells were washed with fresh medium and fixed with 3.5% formaldehyde solution at RT for 10 min. With gentle washing with pure PBS, cells were permeabilized with Triton X-100 0.2% and blocked with

PBS containing 5% FBS. The resulting cells were treated with PBS solution containing rabbit calreticulin polyclonal antibody (dilution ratio 1 : 300, Proteintech Group Inc., Rosemont, IL, USA) and incubated 3 h at 37 °C. Cells were further treated with PBS solution containing Alexa Fluor 488 goat anti-rabbit IgG (H + L) secondary antibody (dilution ratio 1 : 200, Invitrogen, CA, USA) and 3% FBS and incubated 2 h at 37 °C. After washing with pure PBS and staining with 4′,6-diamidino-2-phenylindole (DAPI), cells were observed by using CSLM.

Evaluation of release of HMGB1

CT26 cells were seeded in the glass bottom dish at a density of 3×10^5 cells per dish. After being treated various concentration of T-POS micelles, the cells were incubated for 12 h at 37 °C. Then cells were washed with pure PBS and fixed with 3.5% formaldehyde solution for 10 min. The resulting cells were treated with rabbit anti-*Homo sapiens* (Human) HMGB1 polyclonal antibody (dilution ratio 1 : 200, Cusabio, Houston, TX, USA) and Alexa Fluor 488 goat anti-rabbit IgG (H + L) secondary antibody (dilution ratio 1 : 500, Invitrogen, CA, USA). After that, the release of HMGB1 was monitored using a CLSM.

Evaluation of secretion of ATP

Secretion of ATP was verified by using the EZ-ATP assay kit (DoGenBio Co., Ltd, Korea). CT26 cells were seeded in the 6-well plate at a density of 1×10^6 cells per well. Cells were treated with various concentration of T-POS micelles and incubated for 24 h. Then, the medium on the upper floor was removed, and 100 μL of ATP assay buffer was added to each well. The absorbance of each wells at 570 nm was measured by using a microplate reader to verify the secretion of ATP.

A tumour syngeneic mouse model

To establish a tumour-bearing syngeneic mouse model, CT26 cells (2×10^6 cells per 100 μL) were directly injected into the left flank of normal BALB/c mice (8 weeks old, Orient Bio, Korea), which were randomly divided into four groups. For the biodistribution study, when tumour volume reached approximately 250 mm^3, IR780-loaded T-PCHGE micelles or PCHGE micelles were injected intravenously. Fluorescence images of tumours were captured using a fluorescence bioimaging system (FOBI, Cellgentek, Korea) with a near-infrared (NIR) channel. To evaluate the anticancer activity of T-POS micelles, when tumour volume reached ~50 mm^3, the mice were individually injected intravenously with free OSamp or T-POS micelles (10, 20 mg kg^{-1}) every 3 days. Tumour volumes and body weight were measured for 22 days. All animal experiments were performed in accordance with the Guides for Care and Use of Laboratory Animals of Jeonbuk National University and approved by the Institutional Animal Care and Use Committee (JBNU 2022-069).

Evaluation of *in vivo* immune activation

To evaluate the activation of immune responses, cells were isolated by spleen lysis of untreated mice and T-POS micelles (20 mg kg^{-1})-treated mice. Then, the cells were stained with Alexa Fluor 647 Rat Anti-Mouse CD4 antibody and Alexa Fluor 488 Rat Anti-Mouse CD8a antibody for 3 h. After washing and fixation, the immunofluorescence of resulting cells was measured by using BD FACSymphony A3 (BD Bioscience, CA, USA) to verify the activation of $CD4^+$ T cells and $CD8^+$ T cells.

Histological examination of immunogenic cell death

Tumour tissues of untreated mice and T-POS-treated mice were excised and fixed with 3.5% of formaldehyde for histological evaluation. Tumours were sectioned 5 μm thick and stained with tumour necrosis factor (TNF)-α, CRT or HMGB1 antibody. The fluorescence micrographs of tumour tissues were observed using a CLSM.

Biosafety of T-POS micelles

T-POS micelles were intravenously injected into normal mice at a dose of 100 mg kg^{-1} every other day for 7 days. Blood and organs were collected for chemistry assay and histological examination. The serum level of AL and AST were measured using a kit (Asan Pharm, Korea). The serum levels of BUN and creatinine (Cr) were determined using a kit (Abbex, UK).

Author contributions

G. Kwon: investigation, methodology, writing. J. Baek: methodology. N. Kim: methodology, S. Kwon: methodology, S. Park: conceptualization. B. Kim: conceptualization, funding acquisition, review. D. Lee: conceptualization, funding acquisition, supervision, review, editing.

Conflicts of interest

There are no conflicts to declare.

Acknowledgements

This work was supported by the grant (2020M2D9A3094215, 2021R1A2C3004978) of National Research Foundation of Korea. The authors thank the Center for University-wide Research Facilities (CURF) at Jeonbuk National University for the analysis of confocal laser scanning microscope and mass spectroscopy.

References

1 I. S. Harris, A. E. Treloar, S. Inoue, M. Sasaki, C. Gorrini, K. C. Lee, K. Y. Yung, D. Brenner, C. B. Knobbe-Thomsen, M. A. Cox, A. Elia, T. Berger, D. W. Cescon, A. Adeoye, A. Bruestle, S. D. Molyneux, J. M. Mason, W. Y. Li, K. Yamamoto, A. Wakeham, H. K. Berman, R. Khokha, S. J. Done, T. J. Kavanagh, C.-W. Lam and T. W. Mak, *Cancer Cell*, 2015, **27**, 211–222.

2 W. Yin, J. J. Li, W. D. Ke, Z. S. Zha and Z. S. Ge, *ACS Appl. Mater. Interfaces*, 2017, **9**, 29538–29546.
3 D. Trachootham, Y. Zhou, H. Zhang, Y. Demizu, Z. Chen, H. Pelicano, P. J. Chiao, G. Achanta, R. B. Arlinghaus, J. S. Liu and P. Huang, *Cancer Cell*, 2006, **10**, 241–252.
4 Y. X. Xiong, C. Xiao, Z. F. Li and X. L. Yang, *Chem. Soc. Rev.*, 2021, **50**, 6013–6041.
5 J. Noh, B. Kwon, E. Han, M. Park, W. Yang, W. Cho, W. Yoo, G. Khang and D. Lee, *Nat. Commun.*, 2015, **6**, 6907.
6 E. Austin, E. Koo and J. Jagdeo, *Sci. Rep.*, 2018, **8**, 12599.
7 J. N. Moloney and T. G. Cotter, *Semin. Cell Dev. Biol.*, 2018, **80**, 50–64.
8 M. Nita and A. Grzybowski, *Oxid. Med. Cell. Longevity*, 2016, **2016**, 3164734.
9 S. Bai, L. L. Yang, Y. Wang, T. Zhang, L. Fu, S. Yang, S. Wan, S. Wang, D. Jia, B. Li, P. Xue, Y. Kang, Z. J. Sun and Z. Xu, *Small*, 2020, **16**, e2000214.
10 W. Yan, T. Lang, X. Qi and Y. Li, *Curr. Opin. Biotechnol*, 2020, **66**, 36–43.
11 E. Han, B. Kwon, D. Yoo, C. Kang, G. Khang and D. Lee, *Bioconjugate Chem.*, 2017, **28**, 968–978.
12 N. Song, M. Park, N. Kim, Y. Lee, E. Jung and D. Lee, *Biomater. Sci.*, 2022, **10**, 6160–6171.
13 V. J. Stella, *J. Pharm. Sci.*, 2010, **99**, 4755–4765.
14 H. M. Aliabadi and A. Lavasanifar, *Expert Opin. Drug Delivery*, 2006, **3**, 139–162.
15 Y. Liu, W. Wang, J. Yang, C. Zhou and J. Sun, *Asian J. Pharm. Sci.*, 2013, **8**, 159–167.
16 Y. Z. Du, Q. Weng, H. Yuan and F. Q. Hu, *ACS Nano*, 2010, **4**, 6894–6902.
17 X. Y. Ke, V. W. L. Ng, R. J. Ono, J. M. W. Chan, S. Krishnamurthy, Y. Wang, J. L. Hedrick and Y. Y. Yang, *J. Controlled Release*, 2014, **193**, 9–26.
18 I. Son, Y. Lee, J. Baek, M. Park, D. Han, S. K. Min, D. Lee and B. S. Kim, *Biomacromolecules*, 2021, **22**, 2043–2056.
19 Y. Lee, N. Song, N. Kim, M. Yang, G. Kwon, H. Hyeon, E. Jung, S. C. Park, C. Kim and D. Lee, *Biomacromolecules*, 2022, **23**, 3887–3898.
20 S. Liu, *Mol. Pharm.*, 2006, **3**, 472–487.
21 G. Wang, Z. Wang, C. Li, G. Duan, K. Wang, Q. Li and T. Tao, *Biomed. Pharmacother.*, 2018, **106**, 275–284.
22 Y. Lu, E. S. Zhang, J. H. Yang and Z. Q. Cao, *Nano Res.*, 2018, **11**, 4985–4998.
23 E. Blanco, H. Shen and M. Ferrari, *Nat. Biotechnol.*, 2015, **33**, 941–951.
24 K. Seong, H. Seo, W. Ahn, D. Yoo, S. Cho, G. Khang and D. Lee, *J. Controlled Release*, 2011, **152**, 257–263.
25 K. M. de la Harpe, P. P. D. Kondiah, Y. E. Choonara, T. Marimuthu, L. C. du Toit and V. Pillay, *Cells*, 2019, **8**, 1209.
26 S. Ma, W. T. Song, Y. D. Xu, X. H. Si, S. X. Lv, Y. Zhang, Z. H. Tang and X. S. Chen, *Nano Lett.*, 2020, **20**, 2514–2521.
27 S. Yang, M. K. Shim, W. J. Kim, J. Choi, G. H. Nam, J. Kim, J. Kim, Y. Moon, H. Y. Kim, J. Park, Y. Park, I. S. Kim, J. H. Ryu and K. Kim, *Biomaterials*, 2021, **272**, 120791.
28 J. Fucikova, O. Kepp, L. Kasikova, G. Petroni, T. Yamazaki, P. Liu, L. W. Zhao, R. Spisek, G. Kroemer and L. Galluzzi, *Cell Death Dis.*, 2020, **11**, 1013.
29 B. Montico, A. Nigro, V. Casolaro and J. Dal Col, *Int. J. Mol. Sci.*, 2018, **19**, 594.
30 M. Obeid, A. Tesniere, F. Ghiringhelli, G. M. Fimia, L. Apetoh, J. L. Perfettini, M. Castedo, G. Mignot, T. Panaretakis, N. Casares, D. Metivier, N. Larochette, P. van Endert, F. Ciccosanti, M. Piacentini, L. Zitvogel and G. Kroemer, *Nat. Med.*, 2007, **13**, 54–61.
31 C. Chen, X. Ni, S. R. Jia, Y. Liang, X. L. Wu, D. L. Kong and D. Ding, *Adv. Mater.*, 2019, **31**, 1904914.
32 S. J. He, J. Cheng, X. Feng, Y. Yu, L. Tian and Q. Huang, *Oncotarget*, 2017, **8**, 64534–64550.
33 I. Martins, Y. Wang, M. Michaud, Y. Ma, A. Q. Sukkurwala, S. Shen, O. Kepp, D. Metivier, L. Galluzzi, J. L. Perfettini, L. Zitvogel and G. Kroemer, *Cell Death Differ.*, 2014, **21**, 79–91.
34 J. Y. Zhou, G. Y. Wang, Y. Z. Chen, H. X. Wang, Y. Q. Hua and Z. D. Cai, *J. Cell. Mol. Med.*, 2019, **23**, 4854–4865.
35 Q. Z. Jiang, C. Zhang, H. L. Wang, T. Peng, L. Zhang, Y. Wang, W. D. Han and C. M. Shi, *Front. Oncol.*, 2019, **9**, 1196.
36 B. Li, G. Y. Hao, B. Sun, Z. Gu and Z. P. Xu, *Adv. Funct. Mater.*, 2020, **30**, 1909745.